공학석사학위논문

Development of Precision Structural Analysis for Launch Vehicle Engine Nozzle Sideward Loads

측면하중 예측을 위한 발사체 엔진 노즐 3 차원 고정밀 구조해석 개발

2017 년 8 월

서울대학교 대학원

기계항공공학부

김 세 일

Development of Precision Structural Analysis for Launch Vehicle Engine Nozzle Sideward Loads

측면하중 예측을 위한 발사체 엔진 노즐 3 차원 고정밀 구조해석 개발

지도교수 신 상 준

이 논문을 공학석사 학위논문으로 제출함

2017 년 6 월

서울대학교 대학원

기계항공공학부

김세일

김세일의 석사학위논문을 인준함

2017 년 6 월

위 원 장 김 종 안 (인)

부 위 원 장 신 상 준 (인)

위 원 윤 군 진 (인)

Abstract

Development of Precision Structural Analysis for Launch Vehicle Engine Nozzle Sideward Loads

Seil Kim

Department of Mechanical and Aerospace Engineering

The Graduate School

Seoul National University

In this thesis, an advanced structural analysis is proposed and developed for the prediction of launch vehicle engine nozzle sideward loads. Specifically, the present analysis considers the regenerative cooling channel. The specific elements used are the shell element, which combines the optimal triangle membrane element and discrete Kirchhoff triangle plate bending element. The laminated composite material is considered by improving the existing formulation of the relevant stress-strain relationship. Equivalent structural modeling is conducted considering the outer/inner surfaces and cooling channel of an engine nozzle. The accuracy and efficiency of the shell element are validated by examining both modal and time-transient analyses. The present equivalent structural modeling procedure shows sufficient accuracy when compared with the prediction that takes account of the

original solid element assemblage by considering all the detailed three-dimensional components. To consider the thermal stress in the engine nozzle, the thermomechanical analysis of the engine nozzle is conducted. By conducting the fluid-structure interaction analysis based on the present structural modeling, accurate predictions for launch vehicle engine sideward loads will be anticipated.

Keywords : Structural analysis, Launch vehicle engine nozzle, Sideward loads, Equivalent structural modeling, OPT-DKT facet shell element

Student Number **: 2015-22732**

Table of Contents

List of Figures

List of Tables

List of Symbols

Symbols	Meaning
U_{sh}	Strain energy of an isotropic structure
U_{ls}	Strain energy of the longitudinal stiffeners
U_{or}	Strain energy of an orthotropic shell
T_{sh}	Kinetic energy of an isotropic structure
T_{ls}	Kinetic energy of the longitudinal stiffeners
T_{or}	Kinetic energy of an orthotropic shell
E_i, G_{xs}	Elasticity moduli related to orthotropic shell
ν_i	Poisson's ratio related to orthotropic shell
ν	Poisson's ratio related to isotropic material
D_i	Orthotropic bending stiffness in "i" direction $\frac{t_p^3 E_i}{12\left(1-\nu_x \nu_s\right)}$
D	Isotropic bending stiffness $\frac{t_p^3 E}{12\left(1-\nu^2\right)}$
ρ	Isotropic material density
ρ_{or}	Orthotropic material density
t_p	Shell thickness
A_{ls}	Longitudinal cross sectional area
f_{iso}	Natural frequencies of the stiffened isotropic

	parabolic shell
f_{or}	Natural frequencies of the equivalent orthotropic shell
$\underline{d}_m, \underline{d}_b$	Nodal displacement vector
$u_1, u_2, u_3, v_1, v_2, v_3, w_1, w_2, w_3$	Translational displacements
$\theta_{z1}, \theta_{z2}, \theta_{z3}$	Drilling rotations
$\underline{\underline{k}}_m$	Stiffness matrix of OPT element
$\underline{\underline{k}}_b$	Stiffness matrix of DKT element
$\underline{\underline{k}}_{mb}$	Basic order membrane components
$\underline{\underline{k}}_{mh}$	Higher order membrane components
$E_\circ$	Young's modulus
υ	Poisson's ratio
$\underline{\underline{D}}^e$	Flexural rigidity of the plate
h	Height of the plate
ε_m	Strain of OPT element
ε_b	Strain of DKT element
A	Area of an element
$\underline{N}_x, \underline{N}_y, \underline{N}_{xy}$	Force resultant
$\underline{M}_x, \underline{M}_y, \underline{M}_{xy}$	Moment resultant
$\underline{\underline{A}}^e$	Extensional stiffness matrix
$\underline{\underline{B}}^e$	Membrane-bending coupling stiffness matrix

Chapter 1

Introduction

1.1 Background and Motivation

Advances in high-altitude performance of the launch vehicle engine nozzle requires high-expansion ratio. On the other hand, high expansion ratios result in over-expanded flow condition at sea-level altitude. During the startup and shutdown of the space launch vehicle engines, the engine nozzle operates in an over-expanded condition. Under this condition, when the axial momentum of the flow is larger than that of the radial momentum, the flow will separate from the wall and continue as a free stream, which is called as the free shock separation (FSS). As the chamber pressure increases, internal shock will interact with the Mach wave, and then the separated flow will be re-attached to the wall, which is called as the restricted shock separation (RSS). During the transition from FSS to RSS, an asymmetric pressure distribution will be created by the asymmetric flow separation. This condition will create the transient sideward loads, which causes the elastic deflection of the engine nozzle wall by the fluid-structure interaction. Furthermore, because most of the launch vehicle engine nozzle walls are composed of thin-walled structures, the sideward loads may severely affect engine

components like the gimbal block, actuator, and stiffener. Moreover, it may cause the failure of other hardware. There have occurred failures of the rocket engine hardware, caused by the sideward loads, i.e., FASTRAC, SSME, Vulcain, LE-7A, and J-2S. Thus, engine nozzle sideward loads should be considered in the development stage of a new launch vehicle engine nozzle.

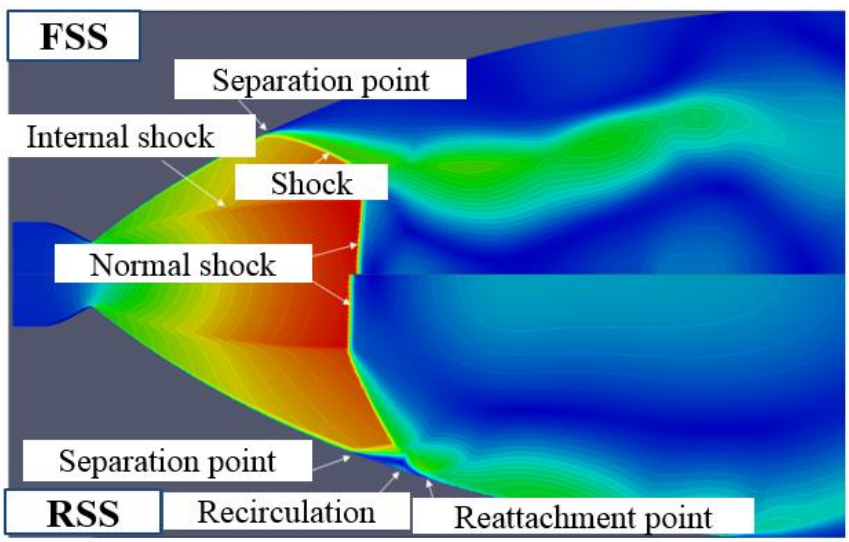

Figure 1.1 Mach contour of FSS/RSS [1]

1.2 Previous Research

In the earlier investigations, Blades [1] conducted an examination of the elastic structural effect in the space shuttle main engine, by going through its fluid-structure interaction analysis. In its structural analysis, a simplified nozzle configuration and isotropic material properties were used. Furthermore, he tried to match the 3rd and 4th modes by the modification of the uniform elastic modulus, and the 2nd mode by changes of the properties at the mid-span of the nozzle. Ludeke [2] conducted the fluid-structure interaction analysis for ARIANE-5 rocket nozzle section. In his structural analysis, both ANSYS and NASTRAN were used. The nozzle configuration was then simplified by modifying the structural configuration to have equivalent structural modes, comparable with those of the original configuration. Garelli [3] performed the fluid-structure interaction analysis for the start-up ignition phase of a rocket engine nozzle. Both linear elastic structural analysis and CFD using 59,600 wedge and prism grids were employed. The result of the fluid-structural interaction analysis was validated using the thin plate flutter analysis. Zhao [4] conducted the fluid-structure interaction analysis of the engine nozzle of J-2s, and compared those with the analysis of a rigid rocket nozzle. He found significant discrepancies in the peak sideward loads between both analyses. Lefrancois [5] analyzed the sideward loads by the interaction between a shock in motion and nozzle movements. He confirmed that the engine nozzle possessed a particular natural frequency, for which the measured sideward loads greatly increased.

In those previous researches, detailed information about the structural analysis for the launch vehicle engine nozzle was not used. Moreover, by conducting an equivalent structural modeling, the nozzle component was assumed to be composed of isotropic material. However, an engine nozzle was typically designed to be a laminated structure, i.e., inner wall, channel, and outer wall. It consists of multiple sections that each have a different thickness and number of ribs. In the equivalent structure modeling of the launch vehicle engine nozzle, the characteristics of each section should be considered. For more efficient and accurate equivalent structure modeling, an organized process will be required in accordance with the structure. The sideward loads may be generated randomly and locally in the nozzle structure. In the three-dimensional precision structural analysis of the engine nozzle, using the shell element, it is required to consider not only the plate bending degrees of freedom, but also the in-plane rotational degree of freedom. To satisfy these requirements, an organized structural analysis, which consists of appropriate structural elements, and equivalent structural modeling, will be required.

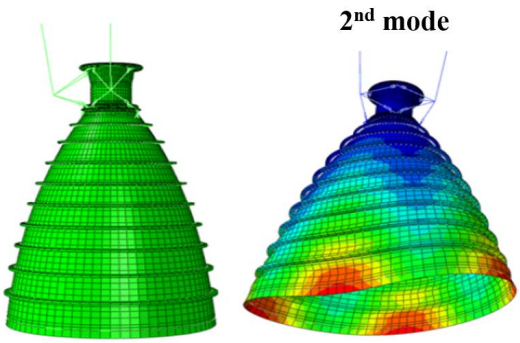

(a) Finite element model and the second mode shape

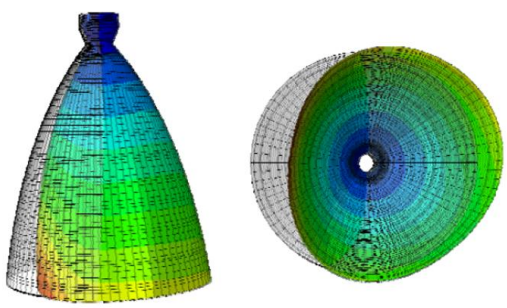

(b) Nozzle deformed shape and deformation contours

Figure 1.2 SSME engine nozzle fluid-structure analysis results [1]

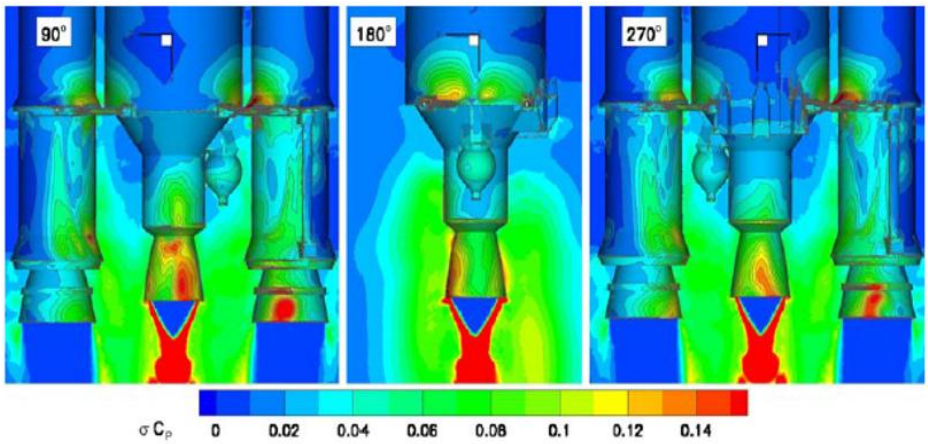

(a) RMS Cp distribution at 32 ms

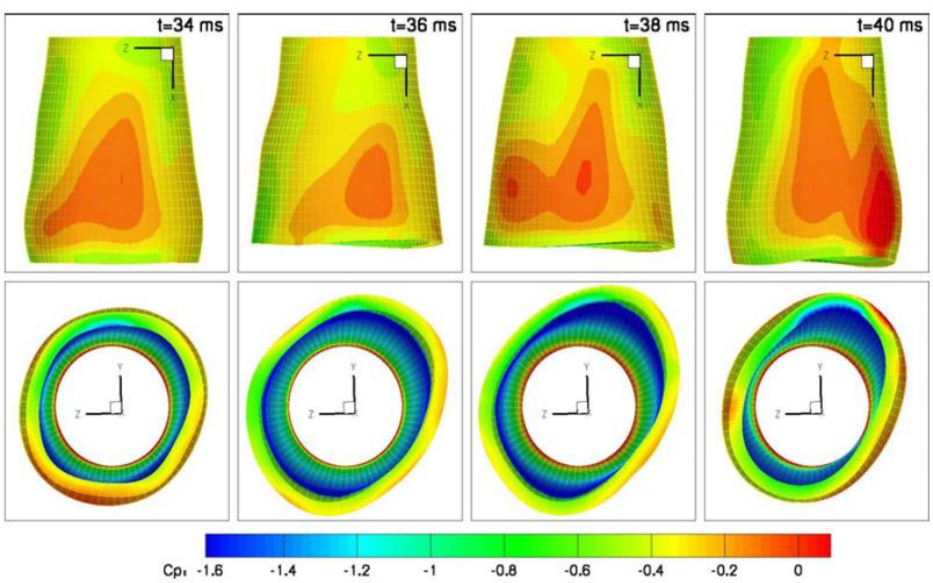

(b) Nozzle deformation, exaggerated view

Figure 1.3 ARIAN-5 nozzle fluid-structure analysis results [2]

1.3 Objectives and Thesis Overview

In this thesis, the structural analysis for the launch vehicle engine nozzle sideward loads is established. The overall process of structural analysis consists of the high-precision OPT-DKT facet shell element and the equivalent structural modeling of the regenerative cooling channel. Three-dimensional structural analysis will be performed using the OPT-DKT facet shell element. This element is created by combining the optimal triangle membrane element (OPT) with the discrete Kirchhoff triangle (DKT) plate-bending element. To consider the transient pressure loads, which are built up later on the engine ignition and may generate sideward loads in the nozzle structure, Newmark time integration method is used in the transient analysis. The laminated composite material is considered by modifying the formulation of the stress-strain relationship, so as to include the membrane-bending coupling effect. To analyze the realistic engine nozzle structure, equivalent structural modeling will be conducted using the shell element and minimization process with orthotropic material properties. Thermal stress will be considered by using thermomechanical analysis.

Chapter 2

Theoretical Background

2.1 Structural Analysis of the Launch Vehicle Engine Nozzle

The analysis of the launch vehicle engine nozzle consists of the high-precision OPT-DKT facet shell element, equivalent structural modeling to consider the regenerative cooling channel and parallel computation.

The present structural analysis framework is shown in Fig. 2.1. To conduct the detailed structural analysis of a launch vehicle engine nozzle, the solid element assemblage, considering the detailed three-dimensional component configuration, needs to be converted into the equivalent shell element assemblage. Moreover, a unique systematic equivalent structural modeling procedure is devised and performed. Based on the equivalent structural modeling, structural analysis is conducted using the OPT-DKT facet shell element. Furthermore, because most of the launch vehicle engine nozzles have similar structural characteristics, this framework will also be applicable to other launch vehicle engine nozzles.

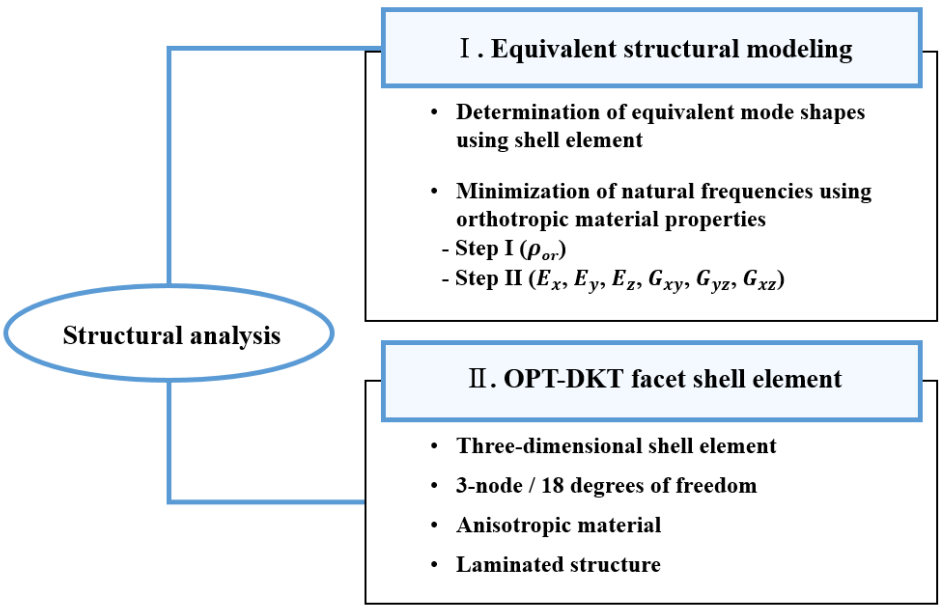

Figure 2.1 Present analysis flowchart for a launch vehicle engine nozzle

2.2 Equivalent Structural Modeling of a Regenerative Cooling Channel using Orthotropic Shell Material Properties

Although the finite element method can be implemented for the complex solid element assemblage that considers the detailed component configuration, it may consume a significant amount of computational time and be inefficient for fluid-structure interaction analysis. By using the shell element, the analysis of a complex structure can be conducted more efficiently. A three-dimensional launch vehicle engine nozzle is usually made up of multiple sections, and is a laminated structure with different thicknesses and numbers of ribs. For its structural analysis using the shell element, an equivalent structural modeling that considers characteristics of each section is required. Additionally, for a more efficient and accurate equivalent structure modeling, an organized procedure is needed.

An analytical process of an equivalent structural modeling for the launch vehicle engine nozzle was established in order to determine the equivalent shell parameters. Most launch vehicle engine nozzle walls are made up of inner layer-regenerative cooling channel-outer layer laminated structures. To conduct structural analysis using the shell element, an equivalent structural modeling of the regenerative cooling channel is required. The equivalent structural modeling is conducted by converting the solid element assemblage, considering the detailed three-dimensional components configuration, to an equivalent shell element assemblage, using the present minimization process with the orthotropic material

properties. The present result is compared with that of the solid element assemblage, in terms of the mode shapes and natural frequencies. The overall process of equivalent structural modeling is simple and applicable to other structures as well. The flowchart of the present equivalent structural modeling is shown in Fig. 2.2.

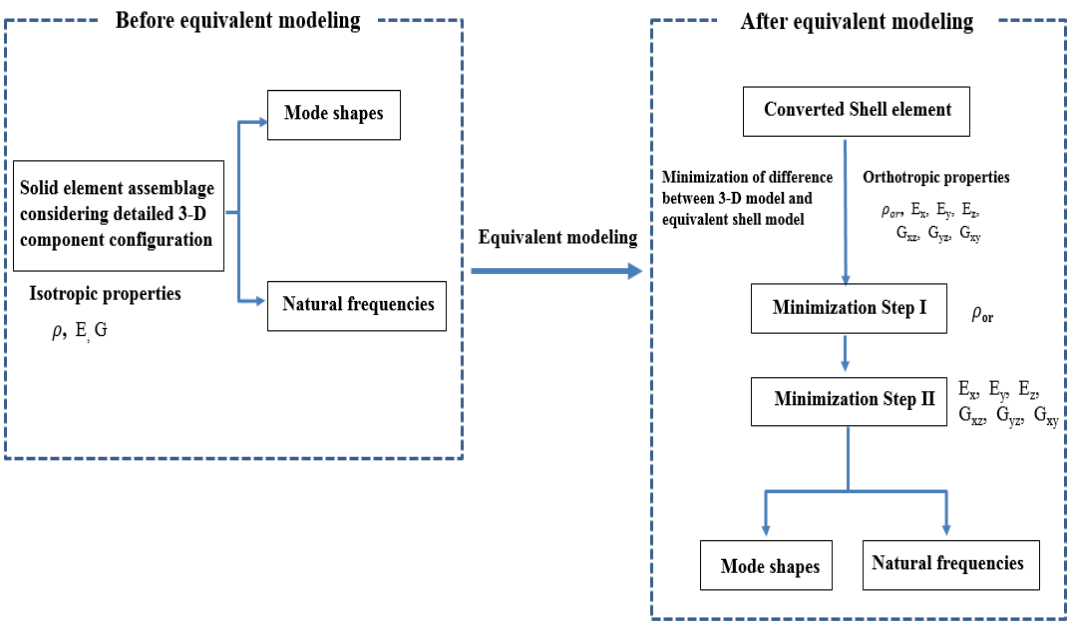

Figure 2.2 Flowchart of the present equivalent structural modeling

Equivalent structural modeling using orthotropic shell material properties

Edalata, et. al. [6] conducted the equivalent structural modeling of a stiffened parabolic structure, using the orthotropic shell parameters. The equivalent orthotropic material properties were obtained using the energy method. Moreover, the concept behind this method assumes that the natural frequencies and mode shapes of the stiffened structure will be the same as those of the orthotropic unstiffened structure. Imposing the equality condition for the energy equations of the stiffened structure and unstiffened orthotropic shell structure, the equivalent orthotropic shell material properties are determined. The strain and kinetic energies for the stiffened curved thin walled structure and unstiffened equivalent structure are written as Eqs. (1)-(6), respectively.

$$U_{sh} = \frac{1}{2}\left\{ D\left[sh(1) + sh(2) \right] + 2\nu D sh(3) + G sh(4) \right\} \tag{1}$$

$$U_{ls} = \frac{E}{2}\left[A_{ls} LS(1) + I_{yy}^{ls} LS(2) \right] + \frac{G}{2} A_{ls} LS(3) \tag{2}$$

$$U_{or} = \frac{1}{2}\left[D_x sh(1) + D_s sh(2) + 2\nu_x D_x sh(3) + G_{xs} sh(4) \right] \tag{3}$$

$$T_{sh} = \frac{1}{2}\rho t_p \left(2\pi f_{iso}\right)^2 sh(5) \tag{4}$$

$$T_{ls} = \frac{1}{2}\rho A_{ls}\left(2\pi f_{iso}\right)^2 LS(4) \tag{5}$$

$$T_{or} = \frac{1}{2}\rho_{or} t_p \left(2\pi f_{or}\right)^2 sh(5) \tag{6}$$

From the equality conditions between the corresponding energy relationships of the stiffened structure and equivalent unstiffened orthotropic shell structure in Eqs. (7)-(10), the equivalent orthotropic material properties, $\rho_{or}, E_x, E_y, E_z, G_{xy}, G_{yz}, G_{xz}$, were extracted [6].

$$U_{iso} = U_{sh} + U_{ls} \tag{7}$$

$$U_{iso} = U_{or} \tag{8}$$

$$T_{iso} = T_{sh} + T_{ls} \tag{9}$$

$$T_{iso} = T_{or} \tag{10}$$

Determination of the equivalent mode shapes using the shell element

The analytical process of equivalent structural modeling for the engine nozzle regenerative cooling channel is established in order to determine the equivalent parameters. The process is divided into the following two procedures: matching mode shapes and minimization of the discrepancies between the predicted frequencies. The equivalent mode shapes were obtained by converting the location of the inner layer and cooling channel that are the stiffened three-dimensional solid element thin walled structure (Fig. 2.3 (a)), into the unstiffened shell element structure (Fig. 2.3 (b)).

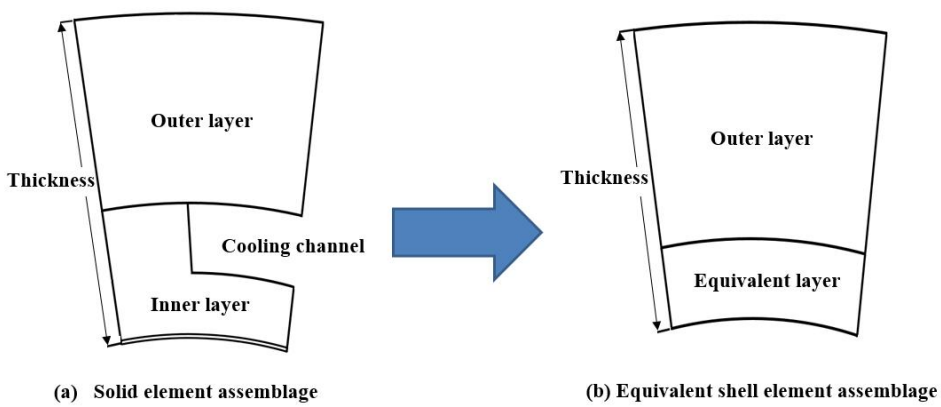

Figure 2.3 Cooling channel cell: the solid element assemblage, considering the detailed 3-D component configuration, and the equivalent shell element assemblage

Minimization of the natural frequency discrepancies using orthotropic material properties

After determination of the equivalent mode shapes, the difference in the natural frequencies between the solid element assemblage considering the detailed three-dimensional component configuration and the equivalent shell element assemblage, is matched using the present minimization process. Furthermore, because the engine nozzle is the elastic component (strain energy≠0), the equivalent natural frequencies are obtained using the variables of energy equations, Eqs. (1)-(10).

In the energy equations, Eqs. (1)-(10), the variables of $\rho_{or}, E_x, E_y, E_z, G_{xy}, G_{yz}, G_{xz}$ are used as the input parameters of the minimization process. For the present minimization process, ANSYS design exploration tool is used. The minimization process is conducted by considering the entire nozzle structure. The minimization process is divided into Steps I and II. In Step I, the natural frequencies of the 1st, 2nd, and 4th mode are to be matched using ρ_{or}, which does not have an effect on the mode shapes. In Step II, the natural frequencies of the 3rd, 5th, and 6th mode are to be matched using $E_x, E_y, E_z, G_{xy}, G_{yz}, G_{xz}$, based on the results of Step I.

A detailed task of the present minimization procedure consists of design of the experiments, response surface, and optimization. In the design of experiments and the response surface, the location of the sampling points is determined using the sparse grid algorithm. The sparse grid algorithm, based on a hierarchy of grids, is a general numerical discretization technique for multivariate problems. The

generation of the sparse grid was based on piecewise multilinear basis functions, which are obtained using a sparse tensor product construction of a one-dimensional multi-level basis. The advantage of this method is that it only refines the required directions. Thus, fewer design points are required for the response surface, to achieve the quality and efficiency necessary to solve the large dimensional problems that have more than 10 uncertain parameters. In the optimization, the multi-objective genetic algorithm (MOGA) is used to consider natural frequencies of the 1^{st}–6^{th} mode, simultaneously. It provides a more refined approach than the screening method does, and is capable of handling multiple goals.

2.3 OPT-DKT Facet Shell Element

In the present structural analysis, the OPT-DKT facet shell element is employed. Felippa [7] developed an optimal triangle membrane element with a drilling degree of freedom, by the construction of an optimal 3-node triangle, using the assumed natural deviatoric strain formulation. Batoz et al. [8] suggested several triangular Kirchhoff plate bending elements, and showed that the discrete Kirchhoff triangle (DKT) would be the most reliable element for the analysis of thin plates. Khosravi [9] developed a new three-node triangular shell element by combining the OPT membrane element and DKT plate bending element. Shape functions of the nine-parameter triangular thin plate bending elements [7] and linear strain triangle 3-node / 9 degree of freedom elements [8] with the same degrees of freedom as that used in the DKT and OPT elements, are used in order to formulate the inconsistent stress and tangent stiffness matrices. Furthermore, the OPT-DKT facet shell element offers good performance for in-plane bending. Using the facet shell element, a total of 18 degrees of freedom (3 translations and 3 rotations at each node) are used to solve the non-linear analysis of thin-walled structures with geometric non-linearity. The facet shell element is different from the conventional shell element in the definition of the inertia matrix, Eq. (13). It is simple to define the degrees of freedom of curved geometry. The degrees of freedom configuration of the OPT-DKT facet shell element is shown in Fig. 2.4.

The vector of the OPT-DKT facet shell element formulated in this paper is rearranged to the membrane and bending degrees of freedom, separately:

$$\begin{Bmatrix} \{\underline{\mathrm{d}}_m\} \\ \{\underline{\mathrm{d}}_b\} \end{Bmatrix} = \begin{Bmatrix} \{u_1\, v_1\, \theta_{z1}\, u_2\, v_2\, \theta_{z2} \cdots \theta_{z3}\}^T \\ \{\omega_1\, \theta_{x1}\, \theta_{y1}\, \omega_2\, \theta_{x2}\, \theta_{y2} \cdots \theta_{y3}\}^T \end{Bmatrix} \tag{11}$$

The stiffness matrix of the shell element corresponding to the displacement vector $\begin{Bmatrix} \{\underline{\mathrm{d}}_m\} \\ \{\underline{\mathrm{d}}_b\} \end{Bmatrix}$ can be described as

$$\underline{\underline{K}} = \int_A \underline{\underline{B_\circ^T D_\circ B_\circ}} dA = \begin{bmatrix} \underline{\underline{K}}_m & \int \underline{\underline{B_m^T B^e B_b}} dA \\ \int \underline{\underline{B_b^T B^e B_m}} dA & \underline{\underline{K}}_b \end{bmatrix} = \begin{bmatrix} \underline{\underline{K}}_m & \underline{\underline{K}}_{mb} \\ \underline{\underline{K}}_{bm} & \underline{\underline{K}}_b \end{bmatrix} \tag{12}$$

The inertial matrix of the OPT-DKT facet shell element can be described as

$$\underline{\underline{M}} = \underline{\underline{E}}_0^T \left[\int_\Omega \rho \underline{\underline{N}}^T \underline{\underline{N}} d\Omega \right] \underline{\underline{E}}_0 \text{, where } \underline{\underline{E}}_0 = diag\left(\underline{\underline{R}}_0, \underline{\underline{R}}_0, \underline{\underline{R}}_0, \underline{\underline{R}}_0, \underline{\underline{R}}_0, \underline{\underline{R}}_0 \right) \tag{13}$$

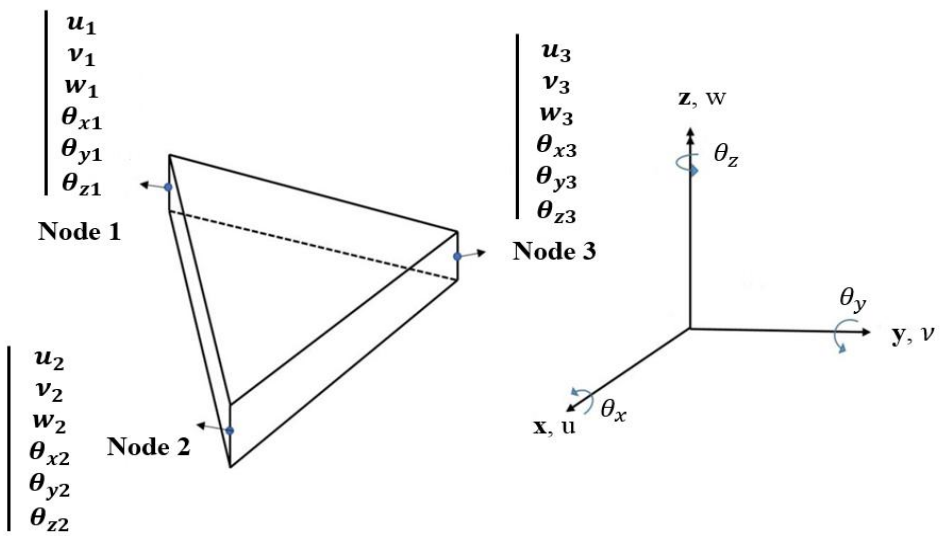

Figure 2.4 Configuration of the OPT-DKT facet shell element

2.4 Extension to Anisotropic Shell Element for Laminated Structures

To consider the laminated composite rocket engine nozzle wall, the formulation of the stress-strain relationship was modified so as to include the membrane-bending coupling effect.

The stress-strain relationship for a thin laminated plate is based on the classical laminated plate theory [9].

$$\begin{Bmatrix} N_x \\ \underline{N}_y \\ \underline{N}_{xy} \\ \underline{M}_x \\ \underline{M}_y \\ \underline{M}_{xy} \end{Bmatrix} = \begin{bmatrix} \underline{\underline{A}}^e & \underline{\underline{B}}^e \\ \underline{\underline{B}}^e & \underline{\underline{D}}^e \end{bmatrix} \cdot \begin{Bmatrix} \varepsilon_x^\circ \\ \varepsilon_y^\circ \\ \gamma_{xy}^\circ \\ \kappa_x^\circ \\ \kappa_y^\circ \\ \kappa_{xy}^\circ \end{Bmatrix} = \begin{bmatrix} \underline{\underline{D}}^\circ \end{bmatrix} \cdot \begin{Bmatrix} \{\varepsilon_m\} \\ \{\varepsilon_b\} \end{Bmatrix} \tag{14}$$

where $\{\varepsilon_m\}$ and $\{\varepsilon_b\}$ are the membrane and flexural strains in the mid-surface of the plate. $\left\{\underline{N}_x \ \underline{N}_y \ \underline{N}_{xy}\right\}^T$ and $\left\{\underline{M}_x \ \underline{M}_y \ \underline{M}_{xy}\right\}^T$ are the resultant force and moment. $\underline{\underline{A}}^e$, $\underline{\underline{B}}^e$ and $\underline{\underline{D}}^e$ are the extensional, membrane-bending coupling and bending stiffness matrices, respectively [9]. The extension-bending coupling stiffness matrix is included in Eq. (14).

2.5 Newmark Implicit Time Integration Method

For the time transient analysis, Newmark implicit time integration scheme is used to obtain accurate predictions at each time step. Newmark integration scheme is based upon an extension of the linear acceleration method, in which it is assumed that the accelerations vary linearly within a time step.

Newmark method consists of the following equations which are used for the determination of three unknowns $\ddot{q}^{t+\Delta t}, \dot{q}^{t+\Delta t}$ and $q^{t+\Delta t}$.

$$M\ddot{q}^{t+\Delta t} + D^{t+\Delta t}\dot{q}^{t+\Delta t} + K^{t+\Delta t}q^{t+\Delta t} = F^{ext^{t+\Delta t}} \tag{15}$$

$$q^{t+\Delta t} = q^{t} + \Delta t\dot{q} + \frac{1}{2}\Delta t^{2}\left(\left(1-2\beta\right)\ddot{q}^{t} + 2\beta\ddot{q}^{t+\Delta t}\right) \tag{16}$$

$$\dot{q}^{t+\Delta t} = \dot{q}^{t} + \Delta t\left(\left(1-\gamma\right)\ddot{q}^{t} + \gamma\ddot{q}^{t+\Delta t}\right) \tag{17}$$

The parameters β and γ will determine the stability and accuracy of the algorithm and are initially proposed by Newmark as $\beta = \frac{1}{4}$ and $\gamma = \frac{1}{2}$.

For linear problems the mass, damping, and stiffness matrices are constant. And the method leads to the repeated solution at each time step giving displacements at time $t + \Delta t$ by solving the system, $K^{eff}q^{t+\Delta t} = F^{eff}$ where the effective quantities are

$$K^{eff} = K + a_0 M + a_1 D \tag{18}$$

$$F^{eff} = F^{ext^{t+\Delta t}} + M\left(a_0 q^t + a_2 \dot{q}^t + a_3 \ddot{q}^t\right) + D\left(a_0 q^t + a_4 \dot{q}^t + a_5 \ddot{q}^t\right) \tag{19}$$

where

$$a_0 = 1/\left(\beta \Delta t^2\right),\ a_1 = \gamma/\left(\beta \Delta t\right),\ a_2 = 1/\left(\beta \Delta t\right),$$
$$a_3 = \frac{1}{2\beta} - 1,\ a_4 = \frac{\gamma}{\beta} - 1,\ a_5 = \frac{1}{2} = \Delta t\left(\frac{\gamma}{\beta} - 2\right),$$
$$a_6 = \Delta t \gamma,\ a_7 = \Delta t\left(1 - \gamma\right)$$

The last two parameters are used for prediction of the accelerations and velocities at time $t + \Delta t$ [19].

$$\ddot{q}^{t+\Delta t} = a_0\left(q^{t+\Delta t} - q^t\right) - a_2 \dot{q}^t - a_3 \ddot{q}^t \tag{20}$$

$$\dot{q}^{t+\Delta t} = \dot{q}^t + a_6 \ddot{q}^t + a_7 \ddot{q}^{t+\Delta t} \tag{21}$$

Chapter 3

Equivalent Structural Modeling

3.1 Equivalent Structural Modeling of a regenerative cooling channel

The launch vehicle engine nozzle is divided into 49 sections. Moreover, each of the sections has a different thickness and number of ribs, as shown in Fig. 3.1. The engine nozzle wall is made up of an inner layer-regenerative cooling channel-outer layer laminated structure, specifically two different materials in the inner layer and two different materials in the outer layer. Figure 3.2 shows the engine nozzle cross-section. The equivalent structural modeling of the regenerative cooling channel is conducted by the determination of the equivalent mode shapes, using the shell element and minimization of natural frequencies with orthotropic material properties. In the determination of the equivalent mode shapes, the location of the inner layer and cooling channel that is the stiffened three-dimensional solid element thin walled structure (Figure 2.3 (a)) is converted to the unstiffened shell element structure (Figure 2.3 (b)), in each section of the nozzle. After the determination of equivalent mode shapes, the natural frequencies are matched using the minimization process. Furthermore, because the engine nozzle is an elastic

component (strain energy $\neq 0$), the equivalent natural frequencies can be obtained using the variables of energy method equations, Eqs. (1)-(10).

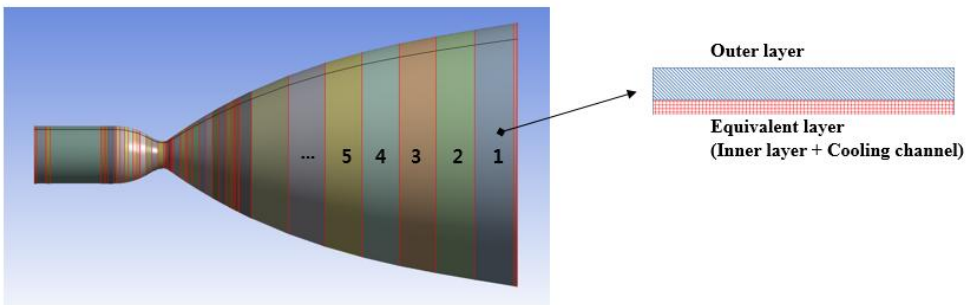

Figure 3.1 Configuration of three-dimensional engine nozzle and converted layer of the nozzle wall

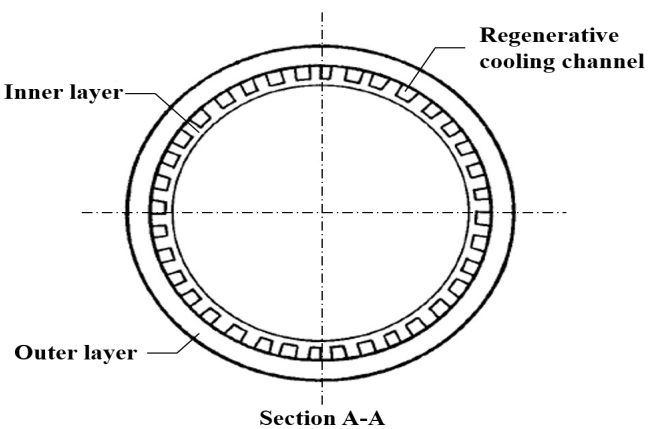

Figure 3.2 Launch vehicle engine nozzle cross-section

Table 3.1 Normalized isotropic parameters of the launch vehicle engine nozzle

Classification	Material A (Inner layer)	Material B (Inner layer)	Material C (Outer layer)	Material D (Outer layer)
E	E_A	E_B	E_C	E_D
ν	ν_A	ν_B	ν_C	ν_D
ρ_{Iso}	ρ_A	ρ_B	ρ_C	ρ_D
G	G_A	G_B	G_C	G_D

Table 3.2 Normalized equivalent orthotropic parameters of launch vehicle engine nozzle

Classification	Material A (Inner layer)	Material B (Inner layer)	Material C (Outer layer)	Material D (Outer layer)
E_x	$0.9\,E_A$	$0.9\,E_B$	$0.7\,E_C$	$1.2\,E_D$
E_y	$2.1\,E_A$	$0.9\,E_B$	$0.7\,E_C$	$1.2\,E_D$
E_z	E_A	E_B	$0.8\,E_C$	$1.3\,E_D$
$\nu_{xy}, \nu_{yz}, \nu_{xz}$	ν_A	ν_B	ν_C	ν_D
ρ_{or}	$0.5\,\rho_A$	$0.4\,\rho_B$	$0.9\,\rho_C$	$0.1\,\rho_D$
G_{xy}	$1.72\,G_A$	$0.9\,G_B$	$0.9\,G_C$	$0.7\,G_D$
G_{yz}	G_A	G_B	G_C	$0.8\,G_D$
G_{xz}	G_A	G_B	G_C	$0.8\,G_D$

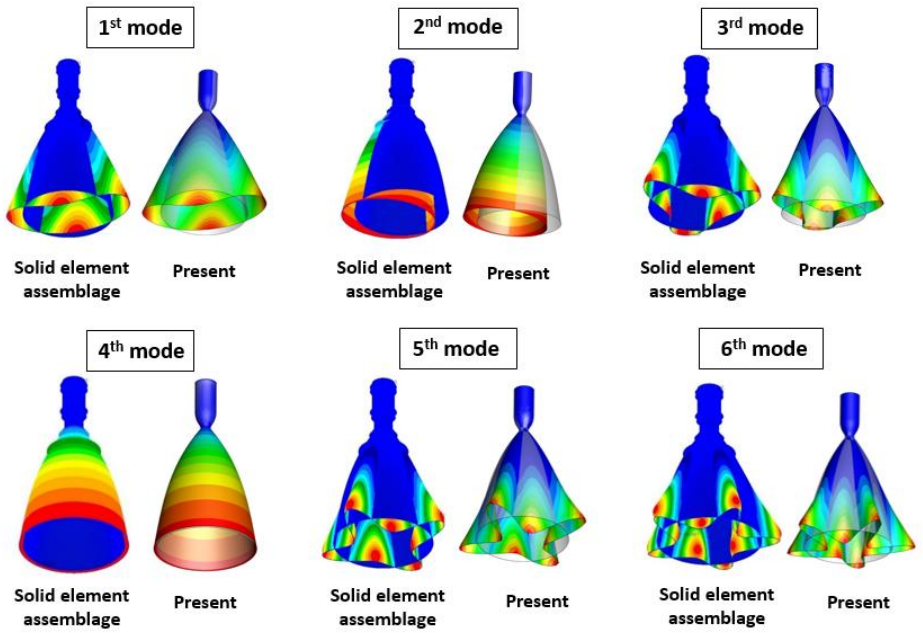

Figure 3.3 Comparison of the mode shapes with the solid element assemblage

Table 3.3 Minimizing discrepancy in the natural frequencies

(a) Before minimization process is applied

Mode	Solid element assemblage (Hz)	Present (Hz)	Diff. (%)
1st	39.8	21.3	16.5
2nd	46	32.4	29.6
3rd	94.1	62.9	33.2
4th	116.8	95.6	18.2
5th	178	125.3	29.6

(b) After minimization process is applied

Mode	Solid element assemblage (Hz)	Present (Hz)	Diff. (%)
1st	39.8	38.6	3.0
2nd	46	43.5	5.4
3rd	94.1	110.9	17.9
4th	116.8	134.5	15.2
5th	178	217.7	22.3

Table 3.4 Comparison of the frequencies with the solid element assemblage

Mode	3-D solid (Hz)	Present (Hz)	Diff. (%)
1st	39.8	38.6	3.0
2nd	46	43.5	5.4
3rd	94.1	110.9	17.9
4th	116.8	134.5	15.2
5th	178	217.7	22.3
		Avg.	12.8

Tables 3.1 and 3.2 summarize the isotropic and equivalent orthotropic parameters of the launch vehicle engine nozzle. Figure 3.3 is the comparison of the present result with the solid element assemblage, considering the detailed three-dimensional component configuration, for the mode shapes of the 1^{st}–6^{th} mode. Table 3.3 shows comparison between the present result and the solid element assemblage, regarding the natural frequencies. The present result (Table 3.3 (b)) shows more improved agreement with those obtained for the solid element assemblage in the 1^{st} – 5^{th} modes, than that shown before the minimization process is applied (Table 3.3 (a)). Table 3.4 shows comparison between the present result and the solid element assemblage, regarding the natural frequencies. The present result shows more improved agreement with that obtained by the solid element assemblage for the 1^{st} – 5^{th} modes. From this systematic equivalent structural analysis process, the complex solid element assemblage, which reflects the detailed component configuration, is successfully converted to the equivalent shell element assemblage. Moreover, the present shell element from the equivalent structural modeling shows improved equivalence for the 1^{st}–5^{th} modes.

Chapter 4

Validation of OPT-DKT Facet Shell Element

4.1 Modal Analysis of the Laminated Anisotropic Material Launch Vehicle Engine Nozzle

Most of the realistic launch vehicle engine nozzle walls are made of laminated composite materials. To analyze such objects, it is assumed that the engine nozzle wall contains anisotropic materials and has a laminated structure: steel-copper-steel. Figure 4.1 shows the three-dimensional launch vehicle engine nozzle configuration and a laminated nozzle wall. The key parameters of the nozzle and analysis conditions are summarized in Table 4.1. Figure 4.2 is the comparison of the present result with NASTRAN, for the mode shapes of the 1^{st} and 2^{nd} mode. Table 4.2 is the comparison between the present result and NASTRAN, regarding the natural frequencies. The present result is in good agreement with that obtained by NASTRAN, within a difference as small as 0.55 % in average.

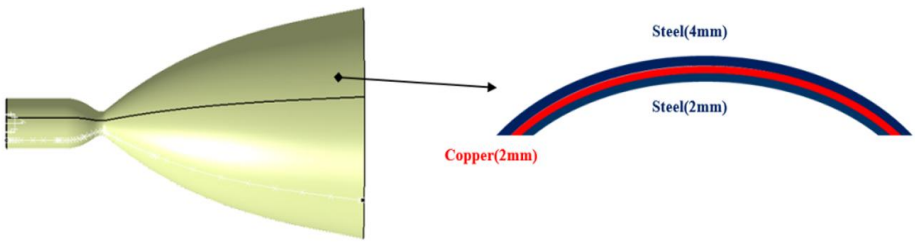

(a) Nozzle configuration **(b) Nozzle wall laminated structure**

Figure 4.1 Three-dimensional launch vehicle engine nozzle

Table 4.1 Parameters of the anisotropic engine nozzle

Classification	Value	Classification	Value (Steel)	Value (Copper)
Total element	12,000	**Elastic modulus**	210 GPa	115 GPa
Total node	6,060	**Poisson ratio**	0.3	0.33
Thickness	8 mm	**Density**	7850 kg/m^3	8860 kg/m^3

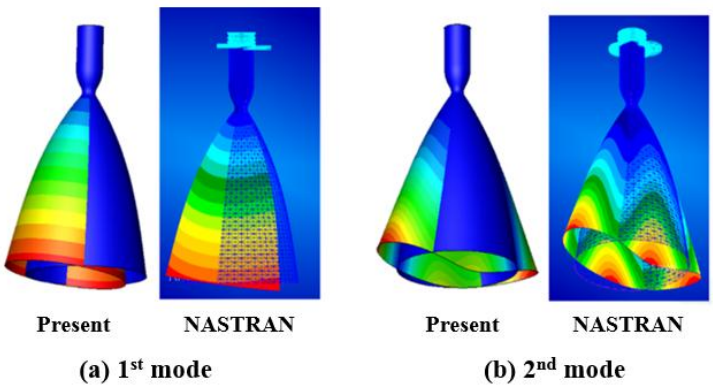

Figure 4.2 Comparison of the mode shapes for an anisotropic engine nozzle

Table 4.2 Comparison of the natural frequencies for an anisotropic engine nozzle

Mode	Present (Hz)	NASTRAN (Hz)	Diff. (%)
1st	23.98	23.78	0.8
2nd	43.98	43.93	0.1
3rd	68.04	67.52	0.8
4th	115.00	114.5	0.4
5th	213.79	211.79	0.9
6th	312.2	311.23	0.3

4.2 Modal Analysis of the Isotropic Material Launch Vehicle Engine Nozzle

Using a simplified liquid rocket engine nozzle configuration, modal analysis was conducted. It is assumed that the nozzle is made by isotropic material and the same thickness. The key parameters of the nozzle and analysis conditions are summarized in Table 4.3. Figure 4.4 is the comparison of the present result with NASTRAN for the mode shapes of the 1st, 2st mode. Table 4.4 is the comparison regarding the natural frequencies between the present result and NASTRAN. The present result showed good agreement with that by NASTRAN within difference as small as 0.55% in average.

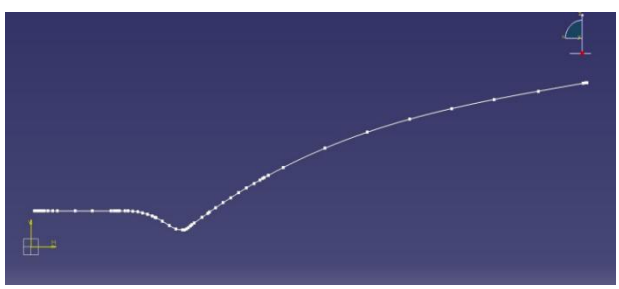

Figure 4.3 2-D configuration of liquid rocket engine nozzle

Table 4.3 Parameters of the isotropic engine nozzle

Classification	Value	Classification	Value (Steel)
Total element	12,000	**Elastic modulus**	210 GPa
Total node	6,060	**Poisson ratio**	0.3
Thickness	8mm	**Density**	7850 kg/m^3

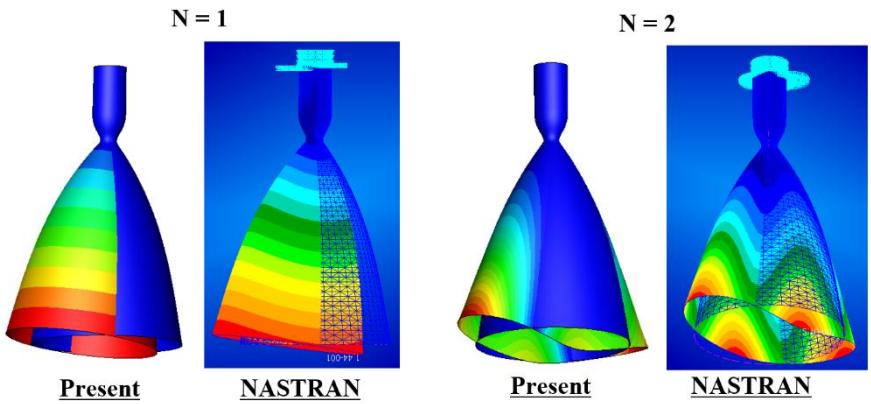

Figure 4.4 Comparison of the mode shapes for the isotropic engine nozzle

Table 4.4 Comparison of the eigenvalues for the isotropic material engine

No	Present (Hz)	NASTRAN (Hz)	Diff. (%)
1	25.66	25.45	0.8
2	45.33	45.29	0.1
3	73.37	72.81	0.8
4	118.51	118.03	0.4
5	220.29	218.33	0.9
6	334.77	333.74	0.3

4.3 Transient Analysis of the Laminated Anisotropic Launch Vehicle Engine Nozzle

Regarding the laminated anisotropic launch vehicle engine nozzle configuration, as shown in Fig. 4.5, the transient analysis is conducted. It is assumed that the nozzle is made of the same thickness. The key parameters of the nozzle and analysis conditions are summarized in Table 4.5. Figure 4.6 is the comparison of the present result with NASTRAN, for the radial displacement at the nozzle tip. The present result is in good agreement with that obtained by NASTRAN, within a difference as small as 1.84% in average.

Table 4.5 Parameters of the anisotropic engine nozzle

Classification	Value	Classification	Value (Steel)	Value (Copper)
Total element	12,000	**Elastic modulus**	210 GPa	115 GPa
Total node	6,060	**Poisson ratio**	0.3	0.33
Thickness	8mm	**Density**	7850 kg/m^3	8860 kg/m^3

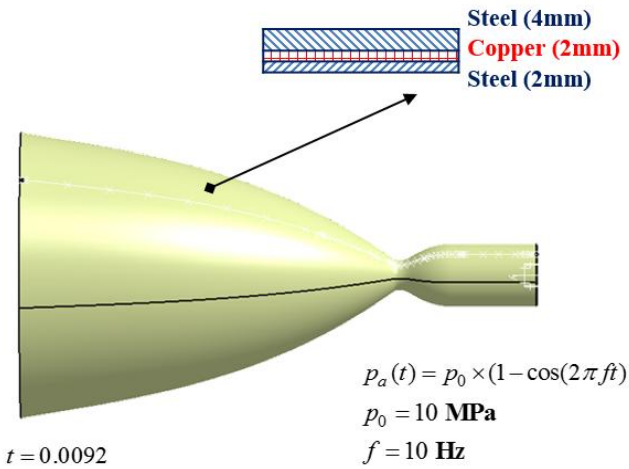

Figure 4.5 Transient analysis input parameters

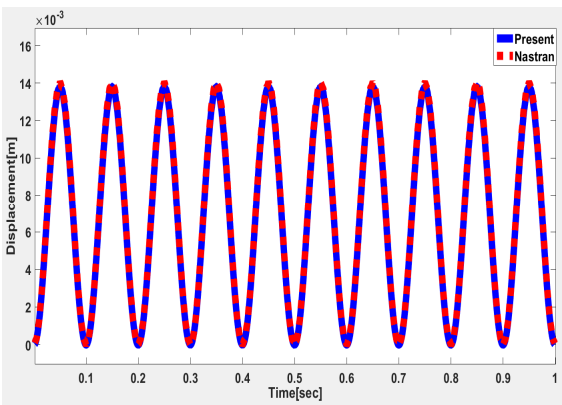

Figure 4.6 Comparison of the radial displacement

4.4 Transient Analysis of the Isotropic Launch Vehicle Engine Nozzle

Using the simplified liquid rocket engine nozzle configuration, transient analysis was conducted. It is assumed that the nozzle is made of isotropic material and the same thickness. The key parameters of the nozzle and analysis conditions are summarized in Table 4.6. Figure 4.8 is the comparison of the present result with NASTRAN for the radial displacement at the nozzle tip. The present result shows good agreement with that by NASTRAN within difference as small as 1.31% in average.

Table 4.6 Parameters of the isotropic engine nozzle

Classification	Value	Classification	Value (Steel)
Total element	12,000	**Elastic modulus**	210 GPa
Total node	6,060	**Poisson ratio**	0.3
Thickness	8mm	**Density**	7850 kg/m^3

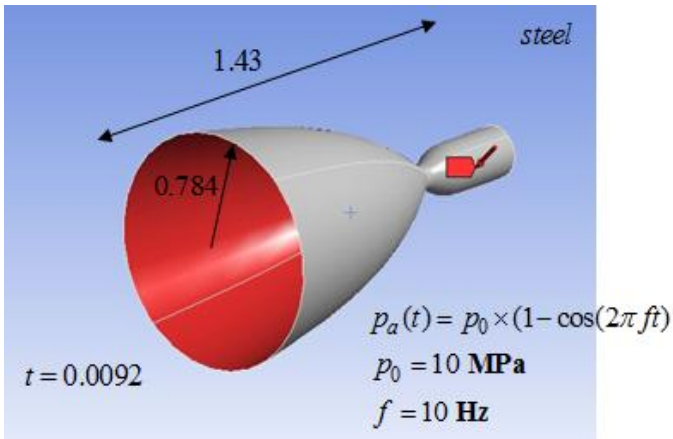

Figure 4.7 Transient analysis input parameters

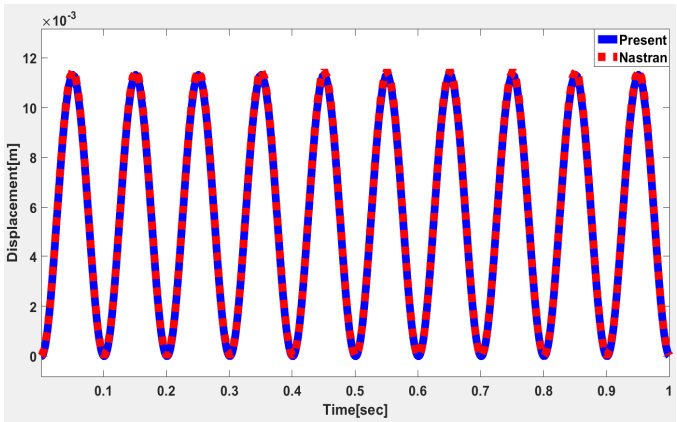

Figure 4.8 Comparison of radial displacement

Chapter 5

Thermomechanical Analysis of an Engine Nozzle

5.1 Thermal Stress Analysis of an Engine Nozzle

Launch vehicle engine nozzle is operated under the high temperature and pressure condition. Temperature of the hot gas flows in the engine nozzle is elevated up to 3,000℃. Under this condition an engine nozzle wall is exposed to extreme thermal loads and the material properties will be varied under the elevated temperature. These thermal loads may generate cracks or severe deflection in the critical area. Thermal-structure interaction analysis is required for these structures which is in the elevated temperature. The failure by the thermal loads, can be predicted by the maximum von Mises stress in the thermomechanical analysis. The engine nozzle wall is usually protected by either thermal barrier coating, film cooling, or regenerative cooling from the thermal loads. Cooling effect should also be considered in the thermal stress analysis for more precise thermal analysis of the structure. Kuhl [20] conducted the coupled heat transfer and stress analysis of a rocket combustion chamber by assuming stationary temperature distribution. In the analysis, plane stress formulation was applied and three dimensional effect was not considered. He analyzed the throat of the nozzle. In this thesis, an analysis of the thermal stress of an engine nozzle is conducted by the thermomechanical analysis using ANSYS software. The process of thermomechanical process of an engine nozzle is shown in Fig. 5.1. The analytical procedure consists of the steady-state

thermal analysis and static structural analysis. The analysis is applied on a critical location of engine nozzle regarding the thermal stress, the throat of the engine nozzle. This area is selected for the present analysis because the highest thermal strains will be created at the area of the highest heat flux [21]. Assuming the stationary temperature distribution, two-dimensional thermal analysis of the cross-section for the engine nozzle is performed. In the thermal analysis, convection in the inner/outer surface of an engine nozzle and conduction in the inner/outer layer of engine nozzle are considered as shown in Fig 5.2. And finally the static structural analysis is conducted based on the result of the thermal analysis.

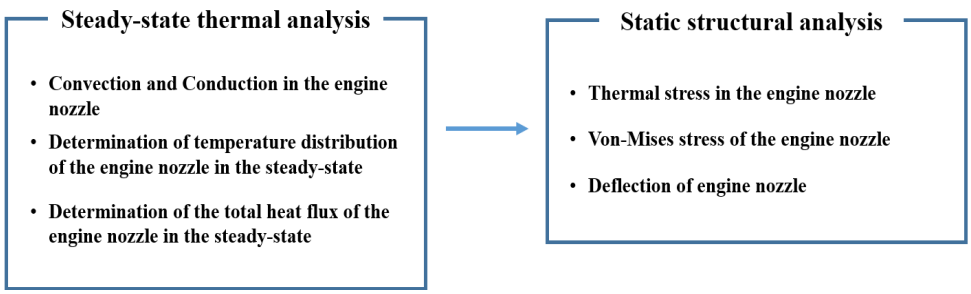

Figure 5.1 Process of the present thermomechanical analysis

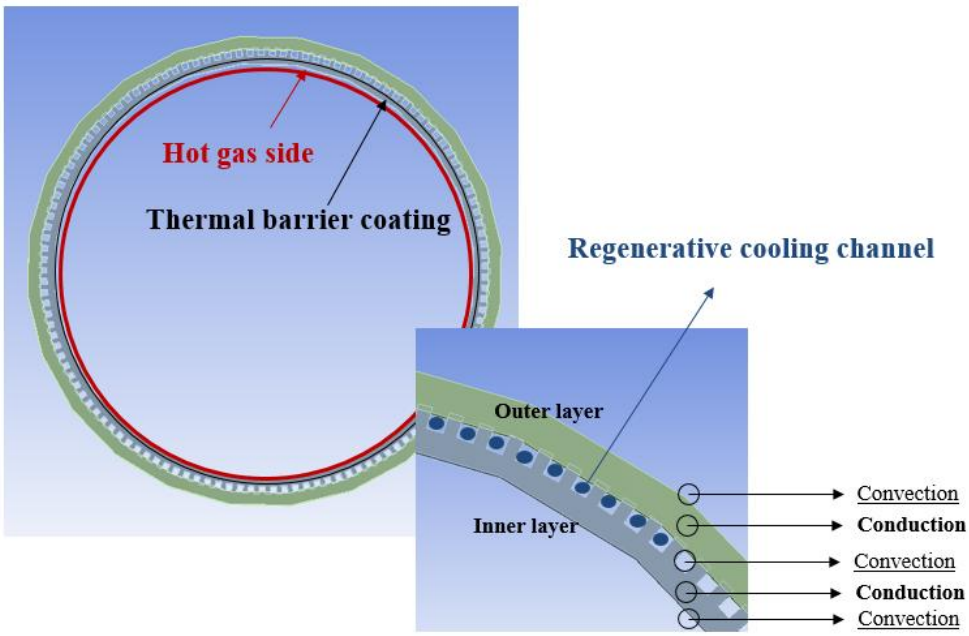

Figure 5.2 Thermal analysis of the cross-section of an engine nozzle

By using the present procedure, the thermomechanical analysis of the throat of engine nozzle is conducted. The inner surface of the nozzle wall is assumed to be 350℃ and coolant (Kerosene) which flows through in the regenerative cooling channel is to be 22℃. The temperature of the nozzle wall in contact with the gases is obtained from the thermal analysis results of the thrust chamber [22]. The analysis result is shown in Fig. 5.3. The present thermal analysis shows the maximum temperature at the throat of the nozzle to be 27.4℃. And the static structural analysis shows the maximum von Mises stress is 21.3 MPa as shown in Figs. 5.4 and 5.5. The portion of the maximum thermal stress is estimated to be 17.2% of the yield strength of Nickel. This framework will also be applicable to other launch vehicle engine nozzles and based on the inner surface of engine

nozzle temperature from the fluid-structure analysis, the thermal stress will be conducted. Finally, the total loads, the combination of thermal effect and pressure will be considered in the structural analysis of an engine nozzle.

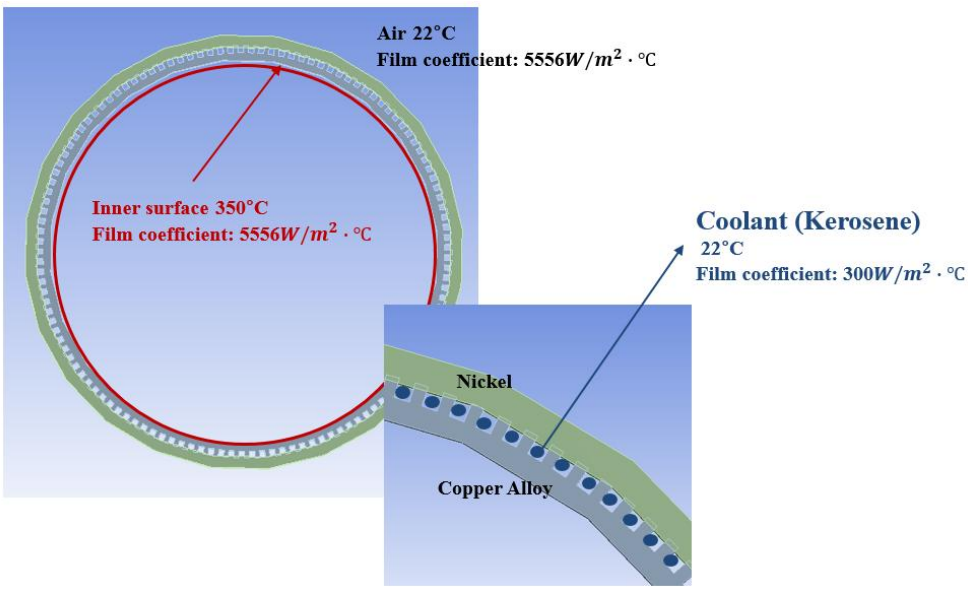

Figure 5.3 Thermal analysis of the cross-section of an engine nozzle

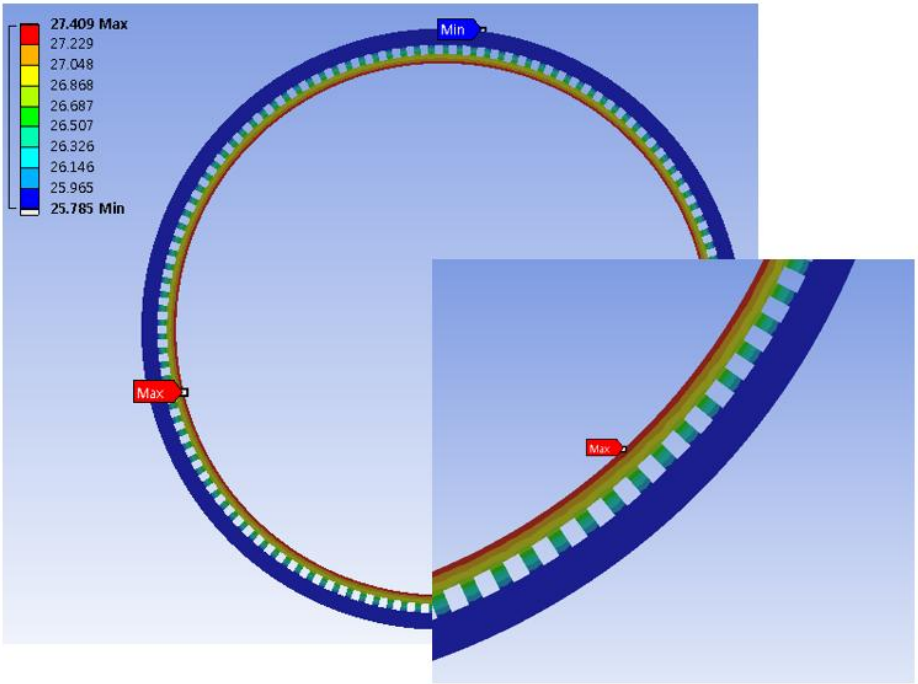

Figure 5.4 Temperature distribution of the present nozzle wall

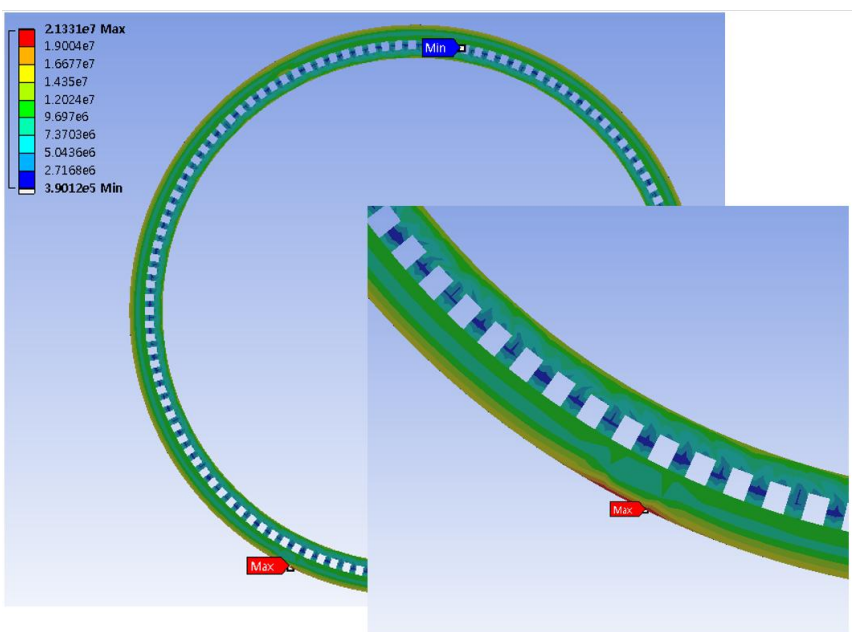

Figure 5.5 Von-Mises stress of the engine nozzle

Chapter 6

Conclusion and Future Works

6.1 Conclusion

In this thesis, a refined structural analysis is established, which will be applicable for the prediction of the launch vehicle engine nozzle sideward loads. The present structural analysis consists of the high-precision OPT-DKT facet shell element, equivalent structural modeling of regenerative cooling channel and parallel computation.

A three-dimensional structural dynamic analysis is performed using the OPT-DKT facet shell element, developed by combining the OPT membrane and the DKT plate bending element. The Newmark time integration method is used for the time transient analysis. The laminated composite material is considered by improving the existing formulation of the stress-strain relationship. Three-dimensional structural analysis for the simplified liquid rocket engine nozzle made of anisotropic material is validated by comparison with the results obtained using NASTRAN. The present result is in good agreement with that obtained using NASTRAN. To analyze the realistic engine nozzle structure, the equivalent structural modeling is conducted using the shell element and minimization process

with orthotropic material properties. The result of the equivalent structural modeling shows improved agreement with the solid element assemblage, considering the detailed three-dimensional component configuration, with the difference of the minimization average before of 34%, and an average afterwards of 8.7%. To consider the thermal stress in the engine nozzle, the thermomechanical analysis of engine nozzle is conducted.

6.2 Future Works

Based on this procedure, the present structural analysis is expected to be coupled with computational fluid analysis, so that it will be capable of considering the detailed fluid-structural interaction in the launch vehicle engine nozzle. Accurate prediction for the sideward loads will then be obtained by conducting such fluid-structure interaction analysis, based on the present structural modeling. Furthermore, the thermal stress analysis capability will be included so that the present analysis will be capable of analyzing the effect of the hot gas around the engine nozzle, and the components under elevated temperatures. The additional details are as follows.

- Fluid-structure interaction analysis of multiple clustering engine nozzles

  In the first stage of the launch vehicle, clustering engine nozzles are used. For the precise fluid-structure interaction analysis of engine nozzle, the interaction between each clustered nozzles should be considered.

- Consideration to the variation of material properties in the elevated temperature

  The material properties will be varied by the elevated temperature. Therefore, variation of each material property should be considered in the overall analysis process.

- Parallel computation of the three-dimensional solid structure.

  The fluid-structure interaction analysis of three-dimensional solid structure analysis can consider the more details of the structure and analyze complex

physical phenomena. The parallel computation will be performed by FETI-local method, the finite element tearing and interconnecting method using the localized Lagrange multiplier. The computational domains are decomposed into non-overlapping sub-domains [22]. The FETI-local method combines the original FETI and its localized Lagrange multipliers [23].

References

[1]Blades, E., Baker, M., Pray, C., and Luke, E., "Fluid-Structure Interaction Simulations of Rocket Engine Side Loads", *SIMULIA Customer Conference*, 2012

[2]Ludeke, H., Calvo, J., and Filimon, A., "Fluid Structure Interaction at the Ariane-5 Nozzle Section by Advanced Turbulence Models," *European Conference on Computational Fluid Dynamics ECCOMAS CFD,* 2006

[3]Garelli, L., Paz, R., and Storti, M., "Fluid-structure interaction study of the start-up of a rocket engine nozzle", *Computers and Fluids,* Vol. 39, 2010, pp. 1208–1218

[4]Zhao, X., Bayyuk, S., and Zhang, S., "Aeroelastic response of rocket nozzles to asymmetric thrust loading," *Computers and Fluids,* 2013, Vol. 76, 2013, pp. 128–148.

[5]Lefrancois, E., "A numerical investigation of side-loads resulting from rigid body motions of an overexpanded engine nozzle," *International Journal for Numerical Method in Fluid*, 2011, Vol. 66, 2011, pp. 671–689

[6]Edalata, P., Khedmati, M. R., and Soares, C. G., "Free Vibration and Dynamic Response Analysis of Stiffened Parabolic Shells using Equivalent Orthotropic Shell Parameters," *Latin American Journal of Solid and Structures*, 2013, Vol. 10, No 4, 2013, pp. 747–766.

[7]Felippa, C. A., "A study of optimal membrane triangles with drilling freedoms," *Computer Methods in Applied Mechanics and Engineering* , Vol. 192, No. 16, 2003, pp. 2125–2168.

[8]Batoz, J. L., Bathe, K. J., and Ho, L. W., "A study of three-node triangular plate bending elements," *International Journal for Numerical Methods in Engineering* , Vol. 15, 1980, pp. 1771–1812.

[9]Khosravi, P., Ganesan, R., and Sedaghati, R., "Corotational non-linear analysis of thin plate and shells using a new shell element," *International Journal for Numerical Methods in Engineering*, Vol. 69, 2007, pp. 859–885.

[17]Allman, J., "Evaluation of the Constant Strain Triangle with Drilling Rotations," *International Journal for Numerical Methods in Engineering*, Vol. 26, 1988, pp. 2645–2655.

[18]Wang, T. S., "Transient Three-Dimensional Analysis of Side Load in Liquid Rocket Engine Nozzles," *40th AIAA/ ASME/SAE/ASEE Joint Propulsion Conference and Exhibit* 11–14 July 2004, Fort Lauderdale, Florida

[19]Stejskal, V., Dehombreux, P., Eiber, A., Gupta, R., and Okhroulik, M., "Mechanics with Matlab," *2011*

[20]Kuhl, D., "Thermomechanical Analysis using Finite Element Methods with Particular Emphasis on Rocket Combustion Chambers," *ECCOMAS 2014*, 2014

[21]Jankovsky, R. S., and Kazaroff, J. M., "A Life Comparison of Tube and Channel Cooling Passages for Thrust Chambers," *NASA Technical Memorandum 103613*, 1990

[22]Choi, H. S., Han, Y. M., Ryu, C. S., and Kim, S. K., "Analytic Consideration of Liquid Rocket Engine Thrust Chamber Design for the KSLV-II," *The Korean Society of Propulsion Engineers 14(4) 71-80*, 2010

[23]Farhat, C., “A method of Finite Element Tearing and Interconnecting and Its Parallel Solution,” *International Journal for Numerical Methods in Engineering*, Vol. 32, 1991, pp. 1205-1227

[24]Kwak, J. Y., Chun, T. Y., and Shin, S. J., “Domain decomposition approach to flexible multibody dynamics simulation,” *Computational Mechanics,* Vol. 53, No. 1, pp. 17-158

국문초록

측면하중 예측을 위한 발사체 엔진 노즐 3 차원 고정밀 구조해석 개발

김 세 일

기계항공공학부

서울대학교 대학원

고고도 비행을 위해 설계된 액체로켓의 경우 지상 연소시험 및 엔진의 초기 연소단계에서 노즐 내부에 과팽창 유동이 발생할 수 있다. 이러한 과팽창 유동은 노즐내부에서 축 방향에 대하여 비대칭 흐름을 야기하고, 이로 인해 발생한 내부 압력 차이에 의해 측면하중이 유도된다. 이러한 유동-구조 상호작용에 의해 발생한 노즐 측면하중은 노즐 구조물의 과도한 변형을 유발하고 고유 진동수 영역과 일치할 경우 엔진 내부에 심각한 구조적 손상을 야기할 수 있어 초기 액체로켓엔진 설계에서 필수적으로 고려되어야 할 요소이다.

본 논문에서는 액체로켓엔진 내부에서 발생할 수 있는 측면하중을 예측하기 위한 3 차원 고정밀 해석 기법을 제시하였다. 구조해석의 구성은 고정밀 OPT-DKT 면 쉘 요소, 재생냉각채널 구조 등가모델링으로 이루어져 있다. Optimal Triangle membrane (OPT) 요소와 Discrete Kirchhoff triangle (DKT) plate bending 요소를 결합한 OPT-DKT 면 쉘 요소를 이용하여 3 차

원 구조해석을 수행하였다. 천이 압력 하중을 고려하기 위해 Newmark 의 시간 전진기법을 사용하였다. 적층된 복합재 구조물의 복합재 형태를 고려하기 위해 응력-변형률 간의 관계식 행렬을 개선하여 membrane-bending coupling 효과가 포함되도록 하였다. 실제 엔진 노즐형상을 고려하기 위해 구조 등가모델링에 대한 프레임워크가 개발되어, 재생냉각채널에 대한 구조 등가모델링이 수행되었다. 고온에 의한 구조 변형 효과 예측을 위한 열-구조 연계 해석의 프레임워크가 개발되었다.

주요어 : OPT-DKT 면 쉘 요소, 로켓엔진 노즐, 노즐측면하중, 적층된 비등방성 재료, 천이 응답 해석, 고유치 해석, 구조 등가모델링

학 번 : 2015-22732